Biomaterials xxx (2009) 1–6

Contents lists available at ScienceDirect

Biomaterials

journal homepage: www.elsevier.com/locate/biomaterials

Magnetic nanoparticles encapsulated into biodegradable microparticles steered with an upgraded magnetic resonance imaging system for tumor chemoembolization

Pierre Pouponneau [a,b], Jean-Christophe Leroux [b,c], Sylvain Martel [a,*]

[a] NanoRobotics Laboratory, Canada Research Chair in Micro/Nanosystem Development, Fabrication and Validation, Department of Computer and Software Engineering and Institute of Biomedical Engineering, École Polytechnique de Montreal (EPM), C.P. 6079, Succursale Centre-ville, Montréal, Québec H3C 3A7, Canada
[b] Canada Research Chair in Drug Delivery, Faculty of Pharmacy, Université de Montréal, Montreal, P.O. Box 6128, Dowtown Station, Montreal, Québec H3C 3J7, Canada
[c] Department of Chemistry and Applied Biosciences, Institute of Pharmaceutical Sciences, ETH Zürich, Wolfgang-Pauli-Str. 10, HCI H 301, 8093 Zürich, Switzerland

ARTICLE INFO

Article history:
Received 23 July 2009
Accepted 2 August 2009
Available online xxx

Keywords:
Magnetism
Nanoparticle
Microencapsulation
MRI (magnetic resonance imaging)
Embolization

ABSTRACT

In this work, therapeutic magnetic micro carriers (TMMC) guided in real time by a magnetic resonance imaging (MRI) system are proposed as a mean to improve drug delivery to tumor sites. MRI steering constraints and physiological parameters for the chemoembolization of liver tumors were taken into account to design magnetic iron–cobalt nanoparticles encapsulated into biodegradable poly(D,L-lactic-*co*-glycolic acid) (PLGA) microparticles with the appropriate saturation magnetization (M_s). FeCo nanoparticles displayed a diameter of 182 nm and an M_s of 209 emu g^{-1}. They were coated with a multilayered graphite shell to minimize the reduction of M_s during the encapsulation steps. FeCo–PLGA microparticles, with a mean diameter of 58 μm and an M_s of 61 emu g^{-1}, were steered in a phantom mimicking the hepatic artery and its bifurcation, with a flow in the same order of magnitude as that of the hepatic artery flow. The steering efficiency, defined as the amount of FeCo–PLGA microparticles in the targeted bifurcation channel divided by the total amount of FeCo–PLGA microparticles injected, reached 86%. The data presented in this paper confirms the feasibility of the steering of these TMMC.

1. Introduction

Hepatocellular carcinoma (HCC), the most frequent primary liver cancer, remains the third cause of cancer-related death [1–3]. The survival rate for 70% of HCC patients relies on the efficacy of palliative treatments [1,2,4]. Trans arterial chemoembolization (TACE), consisting of the injection of chemotherapeutic drugs followed by obstruction of the feeding hepatic arteries supplying the tumor with an embolizing agent, is considered as the mainstay of palliative treatment for unresectable HCC [4–6]. Despite an increase in patients' survival rate, TACE efficacy is limited by the lack of tumor targeting resulting in four main drawbacks: i) a fraction of the injected dose reaches the systemic circulation inducing unwanted cytotoxic effects [7]; ii) the antitumor drug attacks healthy liver cells [4,8]; iii) the procedure remains painful for the patient because healthy blood vessels are embolized [8]; iv) hepatic artery damages can occur during TACE, which can interfere with the catheterization at the next session and compromise the success of the treatment [9]. To minimize TACE drawbacks, we propose the development of therapeutic magnetic micro carriers (TMMC) based on magnetic nanoparticles, which could be steered in real time with an upgraded magnetic resonance imaging (MRI) system from the hepatic artery to HCC nodules and thus to produce a chemoembolization confined to the tumor area (Fig. 1A).

TMMC consist of biodegradable microparticles co-encapsulating an antitumor drug and magnetic nanoparticles required for the MRI steering and tracking (Fig. 1B). After the embolization of tumor blood vessels due to the size of TMMC, the drug will be released as the polymer degrades (Fig. 1A). Thus, the concentration of the drug in the systemic circulation should be reduced and the antitumor effect should be increased by the sustainable release of the drug over time [7,10]. For the steering in the blood vessels, an MRI system upgraded with custom gradient coils placed in its tunnel will be used. The permanent magnetic field of the MRI system saturates the magnetization of nanoparticles [11]. Gradient coils will generate the magnetic force required for the transversal displacement of TMMC in the blood flow to reach the targeted blood vessel (Fig. 1A) and the MRI system will track the position of TMMC.

* Corresponding author. NanoRobotics Laboratory, Department of Computer and Software Engineering and Institute of Biomedical Engineering, École Polytechnique de Montreal (EPM), C.P. 6079, Succursale Centre-ville, Montréal, Québec H3C 3A7, Canada. Tel.: +1 514 340 4711x5098; fax: +1 514 340 5280.
E-mail address: sylvain.martel@polymtl.ca (S. Martel).

0142-9612/$ – see front matter © 2009 Elsevier Ltd. All rights reserved.
doi:10.1016/j.biomaterials.2009.08.005

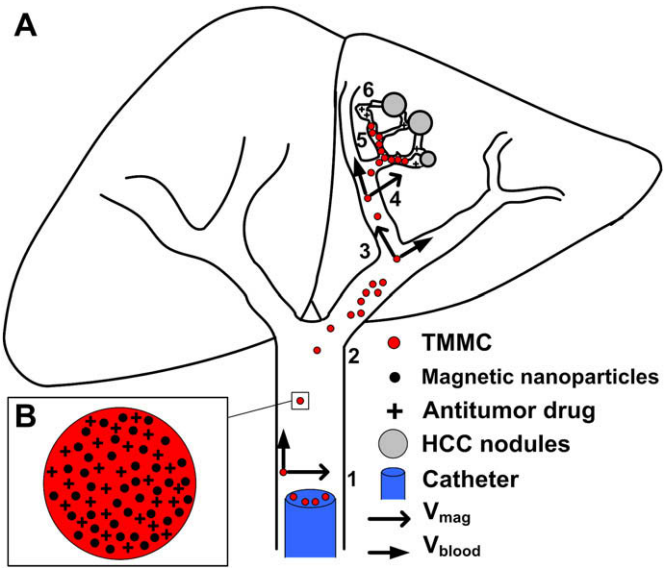

Fig. 1. Schematic representation of the steering of therapeutic magnetic micro carriers (TMMC) for liver chemoembolization: A) Magnetic gradient-controlled steering of TMMC reaching HCC nodules. 1) Release of TMMC from the catheter, 2) Steering of TMMC in the hepatic artery, 3) Steering of TMMC in the left hepatic artery, 4) Steering of TMMC to the tumor blood vessel, 5) Tumor embolization and 6) Drug release. B) Structure of TMMC.

Compared to traditional magnetic drug targeting that uses external magnets to trap magnetic particles and are therefore generally limited to tissues close to the skin [12–16], our technology would control the distribution of TMMC in deep tissues [11,17]. Accordingly, most of TMMC injected could be steered to the tumor area.

This paper introduces the design of TMMC according to MRI steering constraints and physiological parameters. To establish the proof of concept, biodegradable poly(D,L-lactic-*co*-glycolic acid) (PLGA) microparticles loaded with iron–cobalt nanoparticles were successfully steered in a phantom mimicking the hepatic artery (Fig. S1 in the supplementary data).

In this work, the system was designed using physiological parameters of rabbits. This animal model is routinely employed for the assessment of liver tumor treatments [18]. For the embolization of the rabbit liver, 40 μm was reported as the minimum average microparticle diameter [19]. For the MRI steering in the hepatic artery (Fig. 1A), we defined the blood velocity (V_{blood}) as the longitudinal velocity acquired by TMMC dragged by the rabbit hepatic artery blood flow (37 mL/min) [20], and the magnetophoretic velocity (V_{mag}) as the transversal velocity acquired by TMMC under the magnetic gradient in the MRI system [15]. V_{mag} ($m\,s^{-1}$) was calculated according to Equation (1):

$$V_{mag} = \frac{f \times Ms_{nanoparticles} \times \rho \times V_{TMMC} \times \nabla B}{6\pi \times a \times \mu} \quad (1)$$

where, f is the concentration of encapsulated magnetic nanoparticles (% w/w), $M_{s\ nanoparticles}$ is the nanoparticle saturation magnetization ($emu\,g^{-1}$) (emu: electromagnetic units), ρ is the nanoparticle density ($kg\,m^{-3}$), V_{TMMC} is TMMC volume (m^3), ∇B is the applied magnetic steering gradient ($T\,m^{-1}$), a is the TMMC radius (m) and μ is the blood viscosity (0.0035 Pa s). For steering, the hepatic artery was virtually delimited in two areas referred to as areas A and B (Fig. 2A). In order to bring the TMMC *via* the blood flow into the targeted lobe, the TMMC should be in area B at the hepatic artery bifurcation [15]. TMMC, which are in area A, are directed to the targeted lobe by crossing the artery radius (1.25 mm) (Fig. 2A). Accordingly, from V_{mag}, we determined the time required by TMMC to cross the artery radius, referred to as the transit time. We hypothesized that the catheter would be placed at 20 mm from the bifurcation (Fig. 2A), and from V_{blood}, we calculated the time required by TMMC dragged by the blood flow to reach the bifurcation (t_{max}). To reach the targeted lobe, the transit time should be lower than t_{max}. Fig. 2B compares t_{max} to the theoretical transit time calculated for different properties of TMMC – i.e. – TMMC diameter, composition (FeCo vs. Fe_3O_4), loading of magnetic nanoparticles and applied magnetic gradient. It can be seen that compared to Fe_3O_4 nanoparticles ($M_s = 90\ emu\,g^{-1}$) which are used in biomedical applications [13,21,22], FeCo nanoparticles ($M_s = 230\ emu\,g^{-1}$) allow to decrease the loading of nanoparticles in TMMC and decrease the TMMC diameter for a same loading level

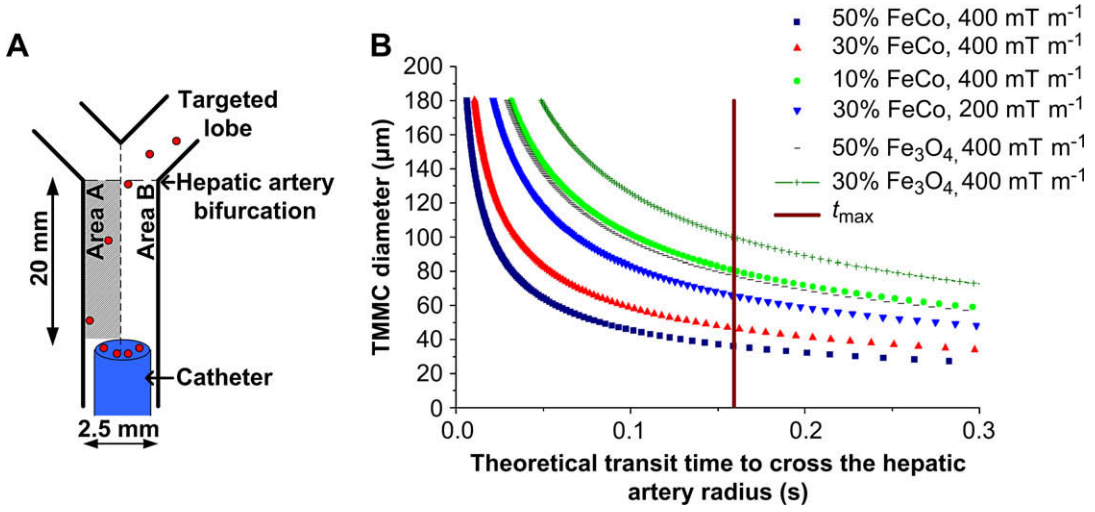

Fig. 2. Design of TMMC for the MRI steering in the hepatic artery of the rabbit: A) Schematic view of the TMMC steering in the rabbit hepatic artery. To reach the targeted lobe, TMMC should end up in area B. The transit time of TMMC to cross the hepatic artery radius should be less than the time required by TMMC dragged by the blood flow to reach the bifurcation (t_{max}) B) Comparison of t_{max} to the theoretical transit time of TMMC required to cross the hepatic radius: influence of composition of encapsulated nanoparticles, nanoparticle loading, TMMC diameter and applied magnetic gradient. For a TMMC diameter of 83 μm, the loading of FeCo nanoparticles is 10% and the loading of Fe_3O_4 nanoparticles is 50%. With a loading 30% of FeCo nanoparticles, TMMC diameter decreases from 70 μm to 50 μm when the magnetic gradient increases from 200 mT m^{-1} to 400 mT m^{-1}.

Please cite this article in press as: Pouponneau P, et al., Magnetic nanoparticles encapsulated into biodegradable microparticles steered with an..., Biomaterials (2009), doi:10.1016/j.biomaterials.2009.08.005

(Fig. 2B) [21,23]. These simulations suggest that under a magnetic gradient of 400 mT m^{-1}, embolization in the targeted hepatic lobe is possible for TMMC bearing 30% FeCo nanoparticles and exhibiting a diameter of 50 μm.

2. Materials and methods

2.1. Materials

$Fe(CO)_5$, oleic acid, tris-*n*-octyl-phosphine oxide, PLGA (M_w = 50,000–70,000; *L*/*G* molar ratio = 50/50), and poly(vinyl alcohol) (PVA, 88% hydrolyzed, M_w = 13,000–23,000) were purchased from Sigma Aldrich (ON, Canada). $Co_2(CO)_8$ and anhydrous dichlorobenzene (DCB) were purchased from Fisher ThermoScientific (ON, Canada). All chemicals and solvents were used without further purification.

2.2. FeCo nanoparticle synthesis

$Co_2(CO)_8$ (1 g) and $Fe(CO)_5$ (1.2 mL) in DCB (12 mL) were cannulated into a solution of oleic acid (1.8 mL) and tris-*n*-octyl-phosphine oxide (0.4 g) in DCB (48 mL) at 200 °C under reflux and inert atmosphere. After 35 min at 285 °C, the suspension was cooled down to room temperature and passed through a 0.2-μm filter (Sigma Aldrich). FeCo nanoparticles were washed three times by centrifugation (45,000*g*, 20 min) with ethanol. FeCo nanoparticles were transferred to a crucible and placed in an oven (Lindberg, MI, USA) under argon atmosphere. The annealing cycle was the following: 20–350 °C at the rate of 11 °C/min maintained for 10 min, 350–650 °C at the rate of 6.5 °C/min maintained for 30 min, 650–250 °C at the rate of 1.5 °C/min. Annealed FeCo nanoparticles were suspended in a solution of oleic acid (7.5 mL) in dichloromethane (DCM) (15 mL). Nanoparticles were sonicated during 6 min at 60 W in pulse mode (Sonic Dismembrator 550, Fisher ThermoScientific) and homogenized with a PowerGen 700D (Fisher ThermoScientific) at 10,000 rpm for 2 min. The sonication and homogenization steps were repeated five times. FeCo nanoparticles were washed three times by centrifugation (15,000*g*, 15 min).

2.3. Encapsulation of FeCo nanoparticles into PLGA microparticles

PLGA (0.37 g) was added to FeCo nanoparticles (0.13 g) in DCM (1 mL). FeCo nanoparticles and PLGA were emulsified (5000 rpm, 5 min) (PowerGen 700D) with an aqueous solution of 0.3% (*w*/*v*) PVA (1.5 mL). At the end of the emulsion step, 0.3% PVA solution (8 mL) was added to the dispersion. DCM was evaporated under rotation in vacuum for 50 min. FeCo–PLGA microparticles were washed three times by centrifugation (1000*g*, 5 min). FeCo–PLGA microparticles were collected on a 20-μm filter. Microparticles were freeze-dried (Freeze Dry system, MI, USA) and stored at −20 °C until use.

2.4. FeCo nanoparticle and FeCo–PLGA microparticle characterization

Before the annealing step, the nanoparticle size in DCM was determined by dynamic light scattering (Zetasizer Nano Series, Malvern Instrument, UK). After the annealing, nanoparticles were imaged by transmission electron microscopy (TEM) (Jeol 2100F, Japan), and the chemical analysis was determined by energy dispersive spectrometry (EDS) (Inca, Oxford Instrument, MA, USA) and atomic absorption spectrometry (AAS) (S Series AAS, Fisher ThermoScientific). AAS was calibrated with Fe and Co standards (Sigma Aldrich). FeCo–PLGA microparticle size distribution was measured by image analysis of data obtained by optical microscopy (Imager Z1, Carl Zeiss GmbH, Germany). FeCo–PLGA microparticles were cut with a focused ion beam (FB-2000A, Hitachi, CA, USA) and the cross-section was imaged by field emission gun scanning electron microscopy (SEM) (Jeol JSM-7600TFE). Magnetic properties of FeCo nanoparticles and FeCo–PLGA microparticles were measured with a vibrating sample magnetometer (VSM) (Walker Scientific, MI, USA) at room temperature. The loading of FeCo nanoparticles was determined by dividing M_s of FeCo–PLGA microparticles by M_s of FeCo nanoparticles before encapsulation. The loading was determined by AAS after degradation of FeCo–PLGA microparticles in a solution of HNO_3 (63 M) and HCl (36 M) at 110 °C under reflux.

2.5. MRI magnetic steering

The MRI steering setup is composed of a 1.5T Siemens Avento clinical MRI scanner (Siemens, Germany), an MRI compatible camera (MRC systems GmbH, Germany) directly above the bifurcation of the phantom, home-made steering gradient coils [11], two syringe pumps (New Era Pump System, Inc., NY, USA), and a Plexiglas hepatic artery phantom with a rectangular cross-section (width = 2.5 mm and depth = 300 μm) (Fig. 1S). The depth of the channel was chosen according to the depth of focus of the camera placed above the bifurcation. An aqueous solution of 3% (*w*/*v*) bovine serum albumin with a viscosity of 0.0015 Pa s (DV-II+ Viscometer, Brookfield, MA, USA) was used. In the phantom, the

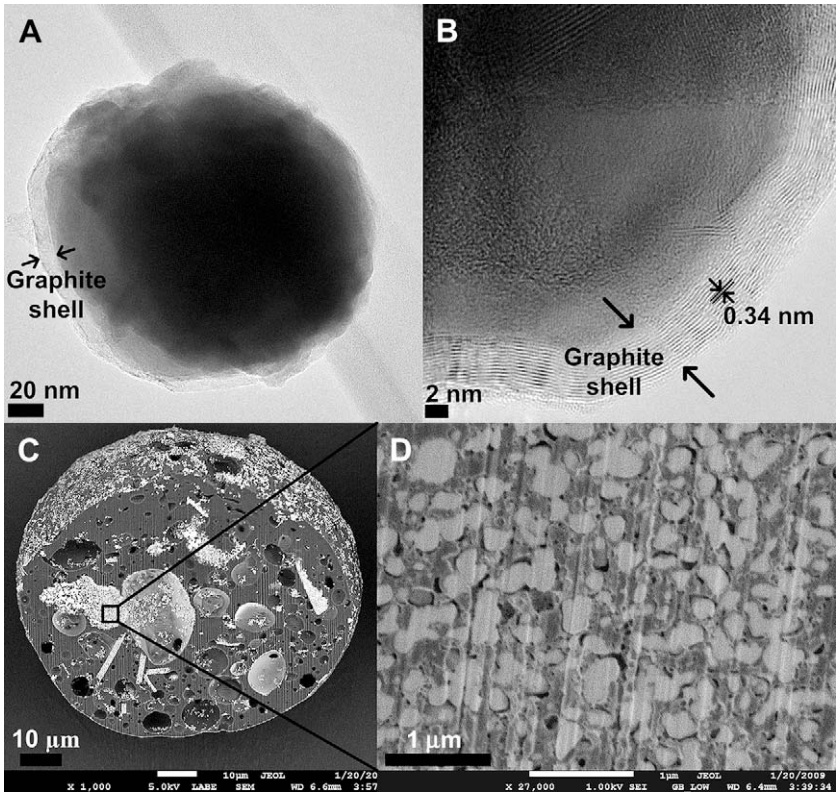

Fig. 3. A) TEM image of FeCo nanoparticles after annealing (scale bar = 20 nm). B) TEM image of the graphite shell of FeCo nanoparticles (scale bar = 2 nm). C) SEM image of the cross-section of FeCo–PLGA microparticle (scale bar = 10 μm). D) FeCo nanoparticle distribution in the PLGA microparticle (scale bar = 1 μm). In Fig. 3c and d, FeCo nanoparticles are white, PLGA are grey and pores are black.

Please cite this article in press as: Pouponneau P, et al., Magnetic nanoparticles encapsulated into biodegradable microparticles steered with an..., Biomaterials (2009), doi:10.1016/j.biomaterials.2009.08.005

flow was set at 8 mL/min (instead of 8.8 mL/min which is the rabbit hepatic artery flow in the phantom) (Fig. S1) [20]. At higher flow, FeCo–PLGA microparticles were not clearly detected by the video camera. The magnetic gradients were +/−400 mT m^{-1} to target each channel outlet (left or right).

The steering efficiency was determined by AAS and video analysis. FeCo–PLGA microparticles collected during each steering assay were degraded in a solution of HNO_3 (63 M) and HCl (36 M). Iron and cobalt concentrations in each vial were quantified by AAS. The steering efficiency was determined by the ratio of the concentration of metallic ions collected in the vial placed at the outlet of the targeted channel divided by the sum of metallic ions collected in the two vials. For the video analysis, the background of each image extracted from steering videos was erased with a MatLab function (The Mathworks, MA, USA). The surface of each aggregate was measured with Zeiss Axiovision software (Carl Zeiss GmbH, Germany). The steering efficiency was determined by the sum of aggregate surfaces in the targeted channel divided by the sum of aggregate surfaces in each channel. The steering results were compared with the Kruskal–Wallis test at 5% confidence level.

3. Results and discussion

3.1. FeCo nanoparticles

FeCo nanoparticles ($d = 15 \pm 8$ nm) were synthesized as described previously [21], and then annealed under inert atmosphere at 650 °C to improve their magnetic properties [24–26]. TEM images show that the mean diameter of annealed FeCo nanoparticles increased to 182 ± 81 nm (Fig. 3A) with a broad size distribution. This could be explained by the aggregation of nanoparticles probably occurring upon the degradation of surfactant during the annealing process. These nanoparticles were coated with a multilayered graphite shell (Fig. 3A and B), with thickness of 8 ± 4 nm and interlayer spacing of 0.34 nm, corresponding to graphite planes [24,26–28]. The atomic ratio (%) Fe:Co in the nanoparticles, determined by EDS and AAS, was 56:44. The saturation magnetization reached 209 ± 1.4 emu g^{-1} (Fig. 4), in agreement with literature [25,28]. M_S remained stable for 7 days, possibly due to the graphite shell which slowed down the oxidation of nanoparticles [26]. Fig. 4 shows that annealed FeCo nanoparticles displayed ferromagnetic behavior because the diameter of nanoparticles allowed the presence of several magnetic domains.

After several sonication and homogenization steps required to suspend FeCo nanoparticles in DCM for their encapsulation into the PLGA microparticles, M_S decreased by 10% (187 ± 6.4 emu g^{-1}) (Fig. 4). However, it remained twice as high as that of Fe_3O_4 nanoparticles. TEM observation (data not shown) suggested that this slight decrease in magnetization was the consequence of the oxidation of some nanoparticles occurring during these steps because some graphite shells were broken.

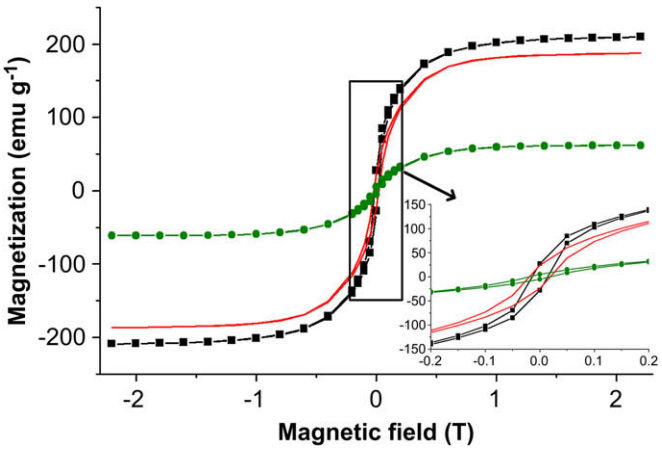

Fig. 4. Hysteresis loops recorded at 20 °C of –■– FeCo nanoparticles after annealing ($M_S = 209 \pm 1.4$ emu g^{-1}), — FeCo nanoparticles before the encapsulation ($M_S = 187 \pm 6.4$ emu g^{-1}), and –●– FeCo–PLGA microparticles ($M_S = 61 \pm 2.5$ emu g^{-1}). Inset shows the hysteresis loop between 0 and 0.2 T.

3.2. FeCo–PLGA microparticles

Fig. 3C shows that FeCo nanoparticles were encapsulated into PLGA microparticles with an average diameter of 58 ± 17 μm (Fig. S2), which fits the size requirement for embolization [19]. According to a cross-section SEM image (Fig. 3C), FeCo–PLGA microparticles were homogenously coated with nanoparticles, whereas the matrix exhibited clusters of closely compacted nanoparticles (Fig. 3D). The loading capacity was estimated at 33% by VSM and at 40% (*w*/*w*) by AAS [29]. This small difference was attributed to the slight decrease of M_S of FeCo nanoparticles because of minor damage to the graphite shell during the encapsulation process. However, the graphite shell prevented a strong decrease of the magnetization due to the sensitivity of FeCo nanoparticles to oxidation during the encapsulation process [24,25,30]. Fig. 4 shows that FeCo–PLGA microparticles displayed a ferromagnetic behavior with an M_S of 61 ± 2.5 emu g^{-1}. To the best of our knowledge, these microparticles exhibited the highest M_S value reported in the literature for magnetic nanoparticles encapsulated into PLGA microparticles [31–34]. The size and the saturation magnetization of FeCo–PLGA microparticles met the steering requirements (Fig. 2B).

3.3. FeCo–PLGA microparticle MRI magnetic steering

The MRI steering ability of the synthesized microparticles was tested in a phantom mimicking the hepatic artery with a flow in the same order of magnitude as that of the hepatic artery flow (Fig. S1). In the MRI tunnel, FeCo–PLGA microparticles formed aggregates oriented in the direction of the magnetic field (Fig. 5A; Videos 1–3

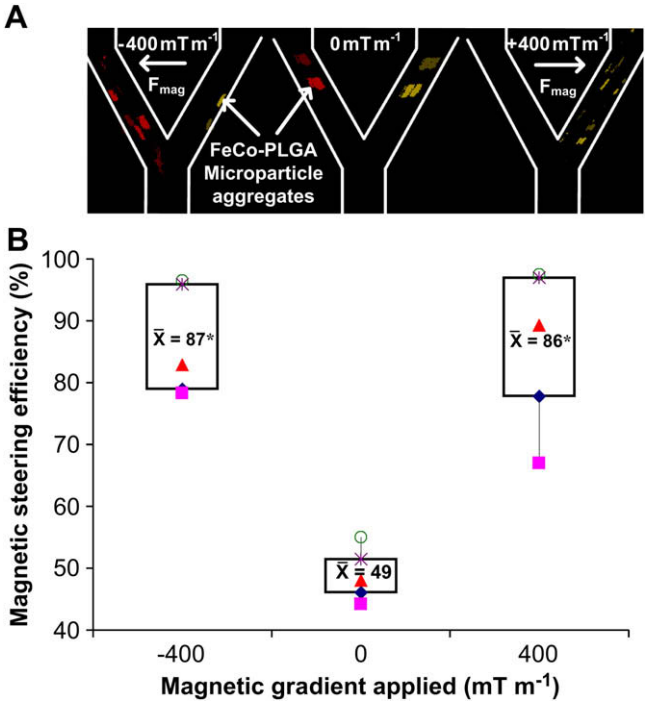

Fig. 5. FeCo–PLGA microparticle steering efficiency: A) Images of FeCo–PLGA microparticle aggregates in the phantom from steering videos after background subtraction. B) Box plots of the in vitro steering efficiency of FeCo–PLGA microparticles. ◆ quartile Q1, ■ minimum, ▲ median, × quartile Q2, ○ maximum. *$p < 0.05$ compared to 0 mT m^{-1} (Kruskal–Wallis test) ($n = 5$ for −400 mT m^{-1}; $n = 3$ for 0 mT m^{-1}, $n = 9$ for 400 mT m^{-1}).

in the supplementary data) [35]. The steering efficiency, defined as the amount of FeCo–PLGA microparticles in the targeted channel divided by the total amount of FeCo–PLGA microparticles in both channels, was determined by AAS and confirmed by video analysis. Fig. 5 shows that without magnetic gradients, FeCo–PLGA microparticles were equally distributed in both channels of the phantom ($49 \pm 5\%$) (Video 1). With a magnetic gradient of $+/-400\ \mathrm{mT\,m^{-1}}$, the steering efficiency reached $86 \pm 11\%$ (Fig. 5, Videos 2 and 3), which represented a significant targeting of the microparticles ($p < 0.05$). The theoretical steering efficiency calculated from V_{mag} reached 73%. As 27% of the volume of the suspension consisted of microparticles smaller than 40 μm, the smallest FeCo–PLGA microparticles could not reach area B before the bifurcation (Fig. 2A). The experimental steering efficiency was found to be greater than the theoretical one due to some magnetic aggregation of FeCo–PLGA microparticles, which increased the magnetic volume to steer [36], thereby reducing transit time (Fig. 2B).

4. Conclusion

FeCo nanoparticles with very high saturation magnetization were successfully encapsulated into PLGA microparticles. The graphite shell surrounding FeCo nanoparticles minimized the M_s loss during the encapsulation process. FeCo–PLGA microparticles exhibited high saturation magnetization required for the MRI magnetic steering and the appropriate mean diameter for the rabbit liver embolization. The magnetic steering assay results demonstrated that FeCo–PLGA microparticles could be steered in a channel mimicking the rabbit liver artery. Further work will aim at further optimizing the system in view of an *in vivo* application.

Acknowledgements

This project is supported by the Canada Research Chair program, the Canada Foundation for Innovation, the National Sciences and Engineering Research Council of Canada (NSERC), Fonds Québécois de la Recherche sur la Nature et les Technologies (FQRNT), and the Government of Québec. The author acknowledges Jeanne Leblond (UDM) for her collaboration in the synthesis of FeCo nanoparticles, Genevieve Gaucher (UDM) for her advices regarding the preparation of PLGA microparticles, Sylvie Marceau and Amira Khoury (UDM) for the access to AAS, Pr. David Menard (EPM) for the access to the VSM, Carole Massicotte (EPM) for the access to the oven, Jean–Baptiste Mathieu (EPM) for his help for steering assays, Charles Tremblay (EPM) for his collaboration in the realization of the phantom, Jean–Philippe Masse (EPM) for his collaboration with TEM analysis, Centre Hospitalier Universitaire de Montreal (CHUM) for the access to the MRI system.

Appendix

Figures with essential colour discrimination. Many of the figures in this article are difficult to interpret in black and white. The full colour version can be found in the on-line version, at doi:10.1016/j.biomaterials.2009.08.005.

Appendix. Supplementary data

Supplementary data such as figures of the MRI steering setup and FeCo–PLGA microparticle size distribution; videos of FeCo–PLGA microparticle flow with and without magnetic gradient in the MRI tunnel are provided in the on-line version. Supplementary data associated with this article can be found in the on-line version, at doi:10.1016/j.biomaterials.2009.08.005.

References

[1] Cabibbo G, Latteri F, Antonucci M, Craxi A. Multimodal approaches to the treatment of hepatocellular carcinoma. Nat Clin Pract Gastroenterol Hepatol 2009;6:159–69.
[2] Bruix J, Sherman M. Management of hepatocellular carcinoma. Hepatology 2005;42:1208–36.
[3] Capocaccia R, Sant M, Berrino F, Simonetti A, Santi V, Trevisani F. Hepatocellular carcinoma: trends of incidence and survival in Europe and the United States at the end of the 20th century. Am J Gastroenterol 2007;102:1661–70.
[4] Lo CM, Ngan H, Tso WK, Liu CL, Lam CM, Poon RT, et al. Randomized controlled trial of transarterial lipiodol chemoembolization for unresectable hepatocellular carcinoma. Hepatology 2002;35:1164–71.
[5] Llovet JM, Real MI, Montana X, Planas R, Coll S, Aponte J, et al. Arterial embolisation or chemoembolisation versus symptomatic treatment in patients with unresectable hepatocellular carcinoma: a randomised controlled trial. Lancet 2002;359:1734–9.
[6] Llovet JM, Bruix J. Systematic review of randomized trials for unresectable hepatocellular carcinoma: chemoembolization improves survival. Hepatology 2003;37:429–42.
[7] Varela M, Real MI, Burrel M, Forner A, Sala M, Brunet M, et al. Chemoembolization of hepatocellular carcinoma with drug eluting beads: efficacy and doxorubicin pharmacokinetics. J Hepatol 2007;46:474–81.
[8] Wigmore SJ, Redhead DN, Thomson BN, Currie EJ, Parks RW, Madhavan KK, et al. Postchemoembolisation syndrome – tumour necrosis or hepatocyte injury? Br J Cancer 2003;89:1423–7.
[9] Maeda N, Osuga K, Mikami K, Higashihara H, Onishi H, Nakaya Y, et al. Angiographic evaluation of hepatic arterial damage after transarterial chemoembolization for hepatocellular carcinoma. Radiat Med 2008;26:206–12.
[10] Hong K, Khwaja A, Liapi E, Torbenson MS, Georgiades CS, Geschwind JF. New intra-arterial drug delivery system for the treatment of liver cancer: preclinical assessment in a rabbit model of liver cancer. Clin Cancer Res 2006;12:2563–7.
[11] Mathieu J-B, Martel S. Magnetic microparticle steering within the constraints of an MRI system: proof of concept of a novel targeting approach. Biomed Microdevices 2007;9:801–8.
[12] Amirfazli A. Nanomedicine: magnetic nanoparticles hit the target. Nat Nanotechnol 2007;2:467–8.
[13] Duran JD, Arias JL, Gallardo V, Delgado AV. Magnetic colloids as drug vehicles. J Pharm Sci 2008;97:2948–83.
[14] Udrea LE, Strachan NJ, Badescu V, Rotariu O. An in vitro study of magnetic particle targeting in small blood vessels. Phys Med Biol 2006;51:4869–81.
[15] Grief AD, Richardson G. Mathematical modelling of magnetically targeted drug delivery. J Magn Magn Mater 2005;293:455–63.
[16] Rudge SR, Kurtz TL, Vessely CR, Catterall LG, Williamson DL. Preparation, characterization, and performance of magnetic iron–carbon composite microparticles for chemotherapy. Biomaterials 2000;21:1411–20.
[17] Martel S, Mathieu J-B, Felfoul O, Chanu A, Aboussouan E, Tamaz S, et al. Automatic navigation of an untethered device in the artery of a living animal using a conventional clinical magnetic resonance imaging system. Appl Phys Lett 2007;90:114105-3.
[18] Pauser S, Wagner S, Lippmann M, Pohlen U, Reszka R, Wolf KJ, et al. Evaluation of efficient chemoembolization mixtures by magnetic resonance imaging therapy monitoring: an experimental study on the VX2 tumor in the rabbit liver. Cancer Res 1996;56:1863–7.
[19] Bastian P, Bartkowski R, Kohler H, Kissel T. Chemo-embolization of experimental liver metastases. Part I: distribution of biodegradable microspheres of different sizes in an animal model for the locoregional therapy. Eur J Pharm Biopharm 1998;46:243–54.
[20] Davies B, Morris T. Physiological parameters in laboratory animals and humans. Pharm Res 1993;10:1093–5.
[21] Hutten A, Sudfeld D, Ennen I, Reiss G, Hachmann W, Heinzmann U, et al. New magnetic nanoparticles for biotechnology. J Biotechnol 2004;112:47–63.
[22] Cheng FY, Su CH, Yang YS, Yeh CS, Tsai CY, Wu CL, et al. Characterization of aqueous dispersions of Fe_3O_4 nanoparticles and their biomedical applications. Biomaterials 2005;26:729–38.
[23] Reiss G, Hutten A. Magnetic nanoparticles: applications beyond data storage. Nat Mater 2005;4:725–6.
[24] Chaubey GS, Barcena C, Poudyal N, Rong C, Gao J, Sun S, et al. Synthesis and stabilization of FeCo nanoparticles. J Am Chem Soc 2007;129:7214–5.
[25] Wang C, Peng S, Lacroix L-M, Sun S. Synthesis of high magnetic moment CoFe nanoparticles via interfacial diffusion in core/shell structured Co/Fe nanoparticles. Nano Research 2009;2:380–5.
[26] Seo WS, Lee JH, Sun X, Suzuki Y, Mann D, Liu Z, et al. FeCo/graphitic-shell nanocrystals as advanced magnetic-resonance-imaging and near-infrared agents. Nat Mater 2006;5:971–6.
[27] Caiulo N, Yu CH, Yu KMK, Lo CCH, Oduro W, Thiebaut B, et al. Carbon-decorated FePt nanoparticles. Adv Funct Mater 2007;17:1392–6.
[28] Desvaux C, Amiens C, Fejes P, Renaud P, Respaud M, Lecante P, et al. Multimillimetre-large superlattices of air-stable iron–cobalt nanoparticles. Nat Mater 2005;4:750–3.

[29] Deng Y, Deng C, Qi D, Liu C, Liu J, Zhang X, et al. Synthesis of core/shell colloidal magnetic zeolite microspheres for the immobilization of trypsin. Adv Mater 2009;21:1377–82.
[30] Wassel RA, Grady B, Kopke RD, Dormer KJ. Dispersion of super paramagnetic iron oxide nanoparticles in poly(D,L-lactide-co-glycolide) microparticles. Colloids Surf A 2007;292:125–30.
[31] Lee S-J, Jeong J-R, Shin S-C, Kim J-C, Chang Y-H, Lee K-H, et al. Magnetic enhancement of iron oxide nanoparticles encapsulated with poly(D,L-lactide-co-glycolide). Colloids Surf A 2005;255:19–25.
[32] Astete CE, Kumar CSSR, Sabliov CM. Size control of poly(D,L-lactide-co-glycolide) and poly(D,L-lactide-co-glycolide)-magnetite nanoparticles synthesized by emulsion evaporation technique. Colloids Surf A 2007;299:209–16.
[33] Zhou S, Sun J, Sun L, Dai Y, Liu L, Li X, et al. Preparation and characterization of interferon-loaded magnetic biodegradable microspheres. J Biomed Mater Res B Appl Biomater 2008;87:189–96.
[34] Okassa LN, Marchais H, Douziech-Eyrolles L, Herve K, Cohen-Jonathan S, Munnier E, et al. Optimization of iron oxide nanoparticles encapsulation within poly(D,L-lactide-co-glycolide) sub-micron particles. Eur J Pharm Biopharm 2007;67:31–8.
[35] Helgesen G, Skjeltorp AT, Mors PM, Botet R, Jullien R. Aggregation of magnetic microspheres: experiments and simulations. Phys Rev Lett 1988;61:1736.
[36] Darton NJ, Sederman AJ, Ionescu A, Ducati C, Darton RC, Gladden LF, et al. Manipulation and tracking of superparamagnetic nanoparticles using MRI. Nanotechnology 2008;19:395102.

Please cite this article in press as: Pouponneau P, et al., Magnetic nanoparticles encapsulated into biodegradable microparticles steered with an..., Biomaterials (2009), doi:10.1016/j.biomaterials.2009.08.005